Interactions of Aβ25−35 β-Barrel-like Oligomers with Anionic Lipid Bilayer and Resulting Membrane Leakage: An All-Atom Molecular Dynamics Study

ARTICLE *in* THE JOURNAL OF PHYSICAL CHEMISTRY B · FEBRUARY 2011

Impact Factor: 3.3 · DOI: 10.1021/jp107558e · Source: PubMed

4 AUTHORS, INCLUDING:

Zhongwen Chang
KTH Royal Institute of Technology
7 PUBLICATIONS **33** CITATIONS

THE JOURNAL OF PHYSICAL CHEMISTRY B

ARTICLE

pubs.acs.org/JPCB

Interactions of Aβ25−35 β-Barrel-like Oligomers with Anionic Lipid Bilayer and Resulting Membrane Leakage: An All-Atom Molecular Dynamics Study

Zhongwen Chang, Yin Luo, Yun Zhang, and Guanghong Wei*

State Key Laboratory of Surface Physics and Department of Physics, Fudan University, 220 Handan Road, Shanghai, 200433, China

Supporting Information

ABSTRACT: Aβ25−35, a proteolytic fragment of the Alzheimer amyloid beta (Aβ) peptide, is produced in the brains of Alzheimer's patients and retains the neurotoxicity of its full-length counterpart. The formation of pores/channels in membranes has been reported as one of the mechanisms responsible for Aβ25−35 toxicity. In addition, it has been proposed that pore/channel might be formed by the aggregation of Aβ25−35 in membranes into a β-barrel structure. However, the structure of the β-barrel and its perturbation on the ordering of lipid bilayer at atomic level remain elusive. In this study, we have investigated the interactions of three types of preformed Aβ25−35 β-barrels (labeled as barrels A, B, and C) with negatively charged palmitoyloleoylphosphatidylglycerol (POPG) lipid bilayers using all-atom molecular dynamics (MD) simulations. Each type of Aβ25−35 β-barrel consists of eight β-strands with positively charged side chains of lysine residues oriented toward the interior or exterior of the barrel. Barrels A, B, and C have respectively an out-of-register mixed parallel−antiparallel (taken from our previous study), in-register mixed parallel−antiparallel, and in-register antiparallel β-strand arrangements. Simulations have been performed by employing the initial configurations where the β-barrels are fully or partially inserted into the bilayer. On the basis of nine independent 150 ns MD runs for the full-insertion system, we found that barrels A and C slightly affect the local ordering of lipid bilayer, while barrel B perturbs the local structure of membrane and even causes membrane leakage for water by forming nanometer-sized hydrophilic pore when lysine residues on its inner side. Two 100 ns MD simulations on partial-insertion system show that partial insertion of Aβ25−35 β-barrel in the bilayer results in a tendency to stay inside for barrel B. These results suggest that barrel B with Lys residues on its inner side is the most likely Aβ25−35 pore structure leading to membrane leakage. Our MD simulations provide significant insight into the atomic resolution structure of Aβ25−35 β-sheet-rich pores and the membrane disruption mechanism induced by Aβ25−35 amyloid pores.

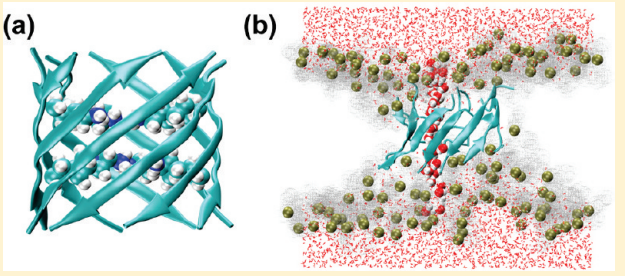

INTRODUCTION

Alzheimer's disease (AD) is the most common neurodegenerative disorder of aging, characterized pathologically by the deposition of amyloid protein plaques. The major components of plaques are amyloid beta (Aβ) peptides, which range in length from 40 to 42 amino acids. These peptides are derived by the proteolytic cleavage of the amyloid precursor protein (APP) by β-secretase at its N-terminus and γ-secretase in the transmembrane region.[1] Aβ can form a variety of different β-sheet-rich aggregates[2] with the soluble oligomers being the most toxic species.[3−5] The mechanism of the toxicity of these oligomeric species has been proposed to be associated with peptide−membrane interactions and the formation of amyloid pores/channels that cause membrane disruption.[6,7] The capacity of Aβ peptides to form pore/channel-like oligomers in a lipid bilayer was originally proposed by Arispe et al.[8,9] The possibility of membrane disruption by Aβ has received additional support by numerous reports of Aβ-induced ion channel activity in artificial and cellular membranes.[10−17] Moreover, the membrane-bound Aβ peptides have been proposed to adopt β-sheet structure[18,19] and can disrupt the membrane severely.[19,20]

Although the full-length Aβ (Aβ1−40 and Aβ1−42) are the major species found in the brains of AD patients, shorter Aβ peptides such as Aβ17−42 and Aβ25−35 have also been observed.[21−23] In particular, Aβ25−35 is an 11-residue peptide produced by enzymatic cleavage of the naturally occurring Aβ1−40.[22] It can cause an increase of membrane permeability and is cytotoxic to neurons.[24−26] The interactions of Aβ25−35 with membranes have been studied extensively by different experimental techniques. Small-angle X-ray diffraction pattern analysis shows that Aβ25−35 is highly lipophilic and inserts into the membrane hydrocarbon core.[27] Neutron diffraction anaysis

Received: August 10, 2010
Revised: December 2, 2010
Published: December 30, 2010

demonstrates that Aβ25−35 inserts quite deeply in the bilayer core of anionic lipid membranes.[28] Several studies by Kagan et al. show that Aβ25−35 can form ion-permeable pores/channels in planar lipid bilayers[24,29,30] and negatively charged lipids increase the channel formation activity.[26] Moreover, Kagan et al. proposed that pore/channel might be formed by the aggregation of Aβ25−35 in membranes into a β-barrel structure.[24,26,29] Inspired by those experimental studies, Ma and Nussinov proposed an all-atom Aβ25−35 pore/channel model based on less than 60 ns molecular dynamics (MD) simulations in the 48th Annual Meeting of the Biophysical Society in 2004.[31] However, an atomically detailed characterization of the pore-/channel-like Aβ25−35 oligomer and its perturbation effects on the anionic lipid bilayer are yet to be determined.

The goal of the present work is to investigate the detailed interactions of preformed Aβ25−35 barrel-like oligomers with the negatively charged palmitoyloleoylphosphatidylglycerol (POPG) lipid bilayer and resulting membrane perturbation. The initial structures of Aβ25−35 oligomers are β-barrels, as proposed by Kagan et al.[24,26,29] Our previous study show that in a polar-hydrophobic environment mixed parallel−antiparallel β-strands have a preference to form β-barrels while purely parallel ones do not,[32] and thus we exclude the purely parallel Aβ25−35 barrel a priori and consider the mixed parallel−antiparallel ones with out-of-register/in-register strand alignment (labeled as barrel A/B). In addition, in-register antiparallel Aβ25−35 β-barrel (labeled as barrel C) is also considered, as β-barrel with antiparallel alignment are regular transmembrane β-barrels (http://www.rcsb.org/pdb/home/). Each β-barrel has two different conformations: one has a hydrophobic pore with Lys residues on its outer side and the other one has a charged hydrophilic pore with Lys residues on its inner side. Thus, six different preformed Aβ25−35 β-barrels are considered in our study. Using extensive molecular dynamics (MD) simulations in a fully solvated explicit POPG lipid bilayer, starting from configurations where the β-barrels are fully or partially inserted into the bilayer, we have studied the details of Aβ25−35-membrane interaction, different effects of barrels A, B, and C on the membrane ordering, membrane permeability for water, the conformational dynamics of Aβ25−35 β-barrel-like oligomers, and their relative stabilities in POPG bilayer.

MATERIALS AND METHODS

Aβ25−35 β-Barrel—Lipid Bilayer System. The sequence of 11-residue Aβ25−35 peptide is G_{25}SNKGAIIGLM$_{35}$. To mimic the experimental neutral pH condition, the side chain of Lys (Lys^+) and the N- and C-termini (NH_3^+, COO^-) are charged. It is known that β-barrels that span the membrane typically comprise 8−22 β-strands (10−13 residues long for each strand).[33] As a first step to explore the interactions of Aβ25−35 β-barrel-like oligomer with POPG membrane, eight-stranded Aβ25−35 β-barrel is taken as a model system in this study. Six different conformations of Aβ25−35 β-barrel (A(out), A(in), B(out), B(in), C(out), C(in)) are used, where "in/out" in the parentheses are for charged Lys residues located on the inner/outer side of the barrel. Barrel A(out) is taken from our previous MD-generated Aβ25−35 β-barrel−carbon nanotube complex in water[32] with the carbon nanotube being removed. This barrel, with most hydrophobic residues protected from aqueous solvent, is characterized by the side chains of Lys located on the outer side of the barrel and a mixed out-of-register parallel−antiparallel arrangement of β-strands. The others are obtained by first constructing a flat eight-stranded β-sheet and then wrapping them into a barrel. Barrel A(in) has the same hydrogen-bond (H-bond) network as A(out) but Lys residues orient toward its interior. Barrel B (B(out) and B(in) for Lys residues on the outside and inside, respectively) has the same mixed parallel−antiparallel β-strand arrangement as barrel A, but different H-bond network (with in-register alignment between strands). Barrel C (including C(out) and C(in) for Lys residues on the outer and inner side of the barrel, respectively) is composed of in-register antiparallel β-strands. The pore diameters of these barrels are 0.3 and ∼0.6 nm for Lys residues on the outside and inside, respectively, calculated by the hole program.[34] The heights of all the barrels are ∼1.7 nm.

The lipid bilayer consists of 2 × 64 POPG lipids (i.e., 64 lipids in each leaflet) and the initial coordinates are obtained from a previous computational study of a pure POPG lipid membrane.[35] The starting configuration for Aβ25−35−membrane system is prepared by inserting the β-barrel into the membrane and removing the overlapping lipid molecules. This has been done by using the INFLATEGRO program implemented by P. Tieleman group.[36] Previous experimental studies by using small-angle X-ray diffraction[27] and neutron diffraction techniques[28] demonstrate that Aβ25−35 inserts quite deeply in the hydrophobic core of lipid bilayer. According to these experimental findings, we insert each barrel fully inside the bilayer to investigate the Aβ25−35 β-barrel−bilayer interactions. The initial configurations of the simulated systems are shown in Figure 1, labeled as A_F(out), A_F(in), B_F(out), B_F(in), C_F(out), and C_F(in) at t = 0 ns, where A, B, and C stand for the three types of β-barrels, respectively, and the subscript F represents the full insertion of the barrel. All the Aβ25−35 β-barrel−bilayer systems are fully solvated in water. Counterions (Na^+) are added to neutralize the system.

Molecular Dynamics Simulations. All the MD simulations have been performed in the isothermal−isobaric (NPT) ensemble using the GROMACS 3.3.1 software package.[37] The protein part of the system is described with the OPLS/AA force field[38] and the POPG lipids with the Berger force field.[39] This combination has been shown to be appropriate for membrane−protein simulations.[40,41] The water is modeled by the simple point charge (SPC) model.[42] Bond lengths of peptides and lipids are constrained with LINCS[43] and water geometries are constrained with SETTLE.[44] This allows an integration time step of 2 fs. Long-range electrostatic interactions are computed using the particle mesh Ewald (PME) method,[45] as recommended for membrane simulations, especially for those involving charged lipids.[46] van der Waals interactions are calculated using a cutoff of 1.4 nm. The temperature of the system is maintained close to 310 K, above the gel−liquid crystal phase transition temperature (271 K) of the POPG membrane,[47] as done recently by Tolokh et al.[48] Lipids, water, peptide, and ions are separately coupled to the temperature bath[49] by weak coupling with a coupling constant of 0.1 ps. The pressure is also weakly coupled (coupling constant of 1.0 ps and compressibility of 4.5 × 10^{-5} bar^{-1}) using semi-isotropic scheme in which the lateral and perpendicular pressures are coupled separately.[36] The reference pressure is 1 bar in all directions, resulting in a bilayer under stress-free condition. All MD simulations are performed using periodic boundary conditions in a rectangular box. In all the systems, the minimum distance between Aβ25−35 β-barrel and the wall of water box is 4.5 nm. Nine independent 150 ns MD

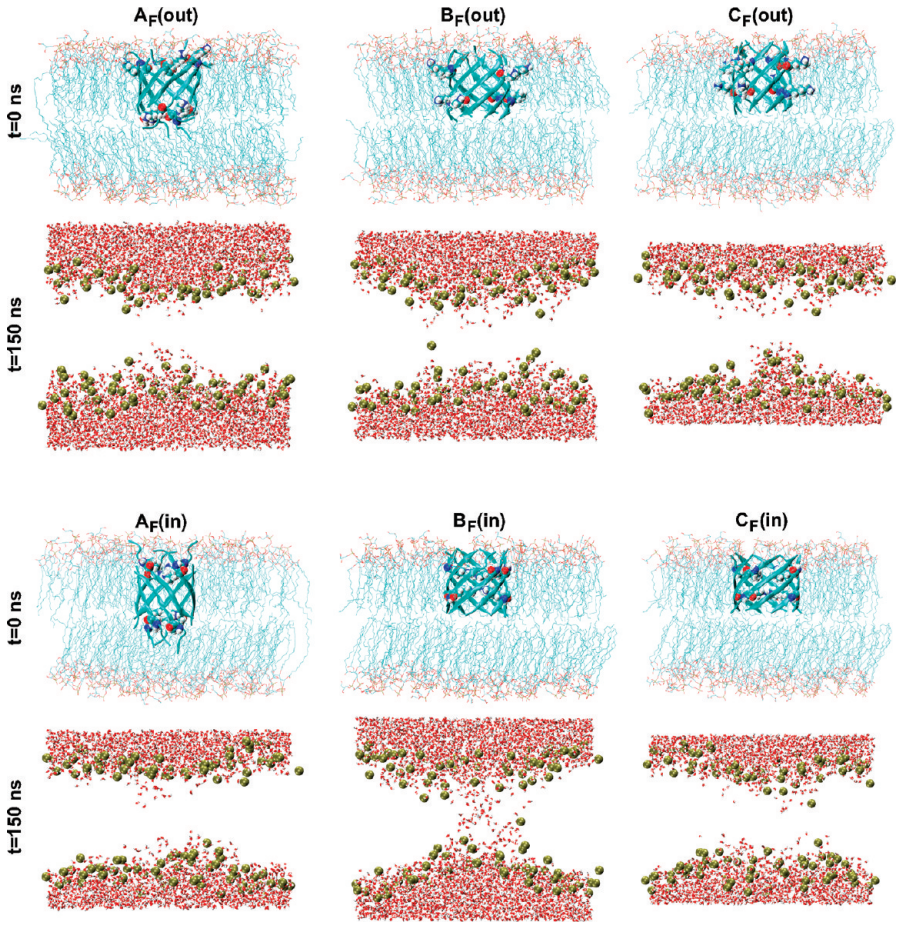

Figure 1. Six initial (t = 0 ns) and final (t = 150 ns) states of all MD runs for full-insertion systems: A_F(out), A_F(in), B_F(out), B_F(in), C_F(out), and C_F(in). Here, A, B, and C stand for the three types of β-barrels, the subscript F for the full insertion of the barrel, and in/out in the parentheses for the position of Lys residues on the inner/outer side of the barrel. In the initial states, for clarity, water molecules are not shown. The heads and tails of POPG lipids are in red and cyan, respectively. Aβ25−35 barrel is shown in cartoon and Lys residues in vdW representation. In the final states (t = 150 ns), the P atoms (tan spheres) of lipids closer to the β-barrel-like oligomer are loosely distributed and water molecules (red dots) are observed in the interior of the POPG bilayer. For clarity, Aβ25−35 β-barrel and the other atoms of POPG bilayer are not shown.

simulations have been performed for each system, starting from the initial state shown in Figure 1.

Analysis. Analyses are performed using tools available in the GROMACS suite. To explore the effect of different barrel on the membrane ordering, we calculate the lipid tail order parameters S_{CD} and the time-averaged angle between lipids and bilayer normal as a function of radial distance from the center of Aβ25−35 barrel. The accumulated number of water molecules across a lipid bilayer and the number of H-bond of Aβ25−35−POPG and of Aβ25−35−water (per peptide chain) are calculated to examine the membrane disruption caused by the three types of β-barrels. In the calculation, water molecule is counted if it enters the bilayer from one side and leaves from the opposite side during the simulations. The conformational dynamics of Aβ25−35 β-barrel are investigated by the time evolution of secondary structure and the number of interpeptide backbone hydrogen bond. The secondary structure calculation uses the DSSP program.[50] One H-bond is considered formed if the distance between N and O is less than 3.5 Å and the angle of N−H···O is greater than 120°. All the systems are displayed using the VMD program.[51]

The relative stabilities of different β-barrels are evaluated based on the Boltzmann probabilities of the barrel-like octamers obtained in our MD simulations, as done recently by Ma and Levine.[52] Monte Carlo simulations are used to estimate the Boltzmann probabilities of different barrel-like octamers based on the conformational energy of the peptide octamers obtained in the last 50 ns of MD simulations. In the calculation of conformational energy of each barrel-like octamer, the effects of water, lipid bilayer, and counterion (Na^+) are also considered. In total 3000 conformations (500 for each of barrel-like octamer examined) are used to calculate the conformational energy. Starting from a randomly selected conformation i, another conformation $i + 1$ was randomly selected from any of the six barrel-like octamers to make conformational move. Then, the Boltzmann factor is used to decide whether it is allowed to move from conformation i to $i + 1$ or not. If $e^{-[(E(i+1)-E(i))/(K_BT)]}$ > random number, the move is accepted; $E(i)$ and $E(i+1)$ are the conformational energies of conformations i and $i + 1$, respectively; K_B is the Boltzmann constant, and T is the temperature (310 K used here). After 1 million trial steps, the conformations visited for each barrel-like octamer are counted. The relative probability of barrel j is evaluated as $P_j = N_j/N_{total}$, where P_j is the population, N_j is the total number of conformations accepted for barrel j, and N_{total} is the total accepted steps.

dx.doi.org/10.1021/jp107558e |J. Phys. Chem. B 2011, 115, 1165–1174

Table 1. Setup Details of all MD Simulations at 310 K[a]

system	name of MD runs	no. of lipid molecules	no. of water molecules	simulation time (ns)	initial state
A_F(out)	A_F1(out), A_F2(out)	126	5237	150	Figure 1 A_F(out)
A_F(in)	A_F3(in)	123	3011	150	Figure 1 A_F(in)
B_F(in)	B_F1(in), B_F2(in), B_F3(in)	124	4419	150	Figure 1 B_F(in)
B_F(out)	B_F4(out)	124	4419	150	Figure 1 B_F(out)
C_F(in)	C_F1(in)	123	3011	150	Figure 1 C_F(in)
C_F(out)	C_F2(out)	123	3011	150	Figure 1 C_F(out)
A_P(out)	A_P1(out)	125	4991	100	Figure 8 A_P(out)
B_P(in)	B_P1(in)	124	5859	100	Figure 8 B_P(in)

[a] For each system, we describe the name of the system, the name of MD runs, the number of lipid and of water molecules, the simulation time, and the initial state of each MD run. To mimic the experimental neutral pH condition, the side chains of Lys (Lys^+), the N- and C-termini (NH_3^+, COO^-) are all charged. Counterions (Na^+) are added to neutralize the system.

RESULTS

To investigate the interactions of Aβ25−35 barrel-like oligomers with a POPG bilayer and resulting membrane disruption as well as the structural dynamics of β-barrel in membrane, a total of 2, 1, 3, 1, 1, 1 MD runs are carried out for A_F(out), A_F(in), B_F(out), B_F(in), C_F(out), and C_F(in) systems, respectively. All MD runs use different initial velocity distributions. A summary of the MD setup details is given in Table 1.

The equilibration of MD simulations is demonstrated by monitoring the time evolution of the interaction energies of Aβ25−35 β-barrel with the solvents (POPG + water) in two independent MD runs for A_F(out) system and in three independent MD runs for B_F(in) system (see Figure S1 in the Supporting Information). The interaction energies reach a plateau after 100 ns in all the MD runs, indicating that our MD simulations have been equilibrated. Similar results are observed for all the other systems (data not shown). Unless specified, the data used in the following analysis are those generated in the last 50 ns of MD simulations.

Full-Insertion of Barrel B Perturbs the Local Membrane Structure and Causes Membrane Leakage. Figure 1 shows the final states (at t = 150 ns) generated in representative MD runs of the six systems A_F(out), A_F(in), B_F(out), B_F(in), C_F(out), and C_F(in). The loosely distributed phosphorus (P) atoms in the head groups of lipids closer to Aβ25−35 barrel-like oligomer demonstrate membrane perturbation takes place locally in all the systems, but the disruptive effect of barrel B is much larger than that of barrels A and C. In addition, water molecules are observed in the hydrophobic center of POPG bilayer in B_F(in) system, while they are trapped in the head groups of lipids and no water molecules are seen in the center of POPG bilayer in all the other systems. Therefore, in the following analysis, we focus on the data generated in the MD runs of B_F(in) system and of A_F(out) system (taking A_F(out) system as representative of other systems).

The final configurations (at t = 150 ns) obtained in all the MD runs of A_F(out) and B_F(in) systems are given in Figure 2. The snapshots in the two independent MD runs A_F1 (out) and A_F2 (out) and those in the three independent MD runs B_F1(in), B_F2(in), and B_F3(in) depict that barrel B(in) perturbs the local structure of membrane more severely than barrel A(out) and causes water molecules penetrating into the hydrophobic center of the POPG bilayer.

To characterize the perturbation effects of barrels A(out) and B(in) on the membrane ordering, we calculate the lipid tail order

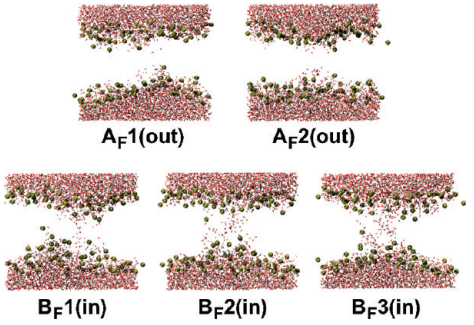

Figure 2. Snapshots at t = 150 ns generated in all the MD runs of A_F(out) and B_F(in) systems. The phosphorus (P) atoms (tan spheres) of lipids closer to the β-barrel-like oligomer are loosely distributed and water molecules (red dots) are observed in the interior of the POPG bilayer. For clarity, Aβ25−35 β-barrel and the other atoms of POPG bilayer are not shown.

parameter S_{CD}, using

$$S_{CD} = 0.5\langle 3\cos^2\alpha - 1\rangle$$

where α represents the angle between the C−H bond vector (in the simulation) or the C−D bond vector (in the experiment) and the bilayer normal. The angular brackets indicate averaging over lipids and over time.[49] Figure 3 gives the order parameters S_{CD} of acyl chain 1 (*sn*-1) of lipids in all the MD runs of A_F(out) and B_F(in) systems. For comparison, the S_{CD} of *sn*-1 from a 100 ns MD run of a pure POPG lipid bilayer is also presented. In this figure, the order parameters of carbon atoms 8−14 in the lipid tail ends are quite similar among all the simulations, while distinct differences exist for carbon atoms 1−6 in the lipid tail heads. In what follows, the order parameters discussed are for carbon atoms 1−6. The S_{CD} values of lipids for A_F(out) system are slightly smaller than those in a pure POPG bilayer. Similar results are obtained in A_F(in), C_F(in), and C_F(out) systems (see Figure S2 in the Supporting Information). In contrast, a bigger decrease of S_{CD} values is observed in B_F system. Moreover, the S_{CD} values in the three MD runs of B_F(in) system are smaller than those in the two MD runs of A_F(out) system. These results suggest that the membrane-embedded barrel B strongly affect the ordering of the lipid tail heads of POPG bilayer.

After investigating the effects of Aβ25−35 β-barrel on the hydrophobic tails of a POPG lipid bilayer, we examine the influences of the two different β-barrel conformations on the orientation of the lipids. The orientation of a lipid is defined by

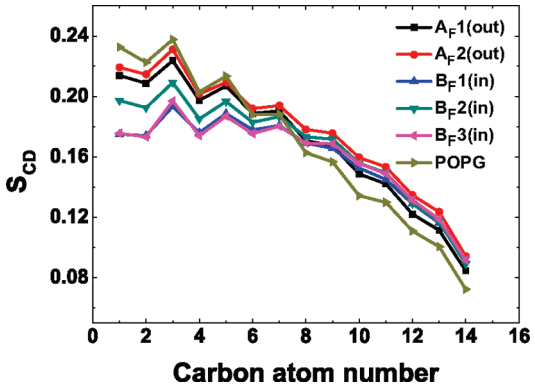

Figure 3. Time-averaged order parameter S_{CD} of *sn*-1 chain of lipids over the last 50 ns of MD trajectory for all the MD runs of A_F(out) and B_F(in) systems. For comparison, the S_{CD} of *sn*-1 obtained from a 100 ns MD run for pure POPG lipid bilayer is also presented.

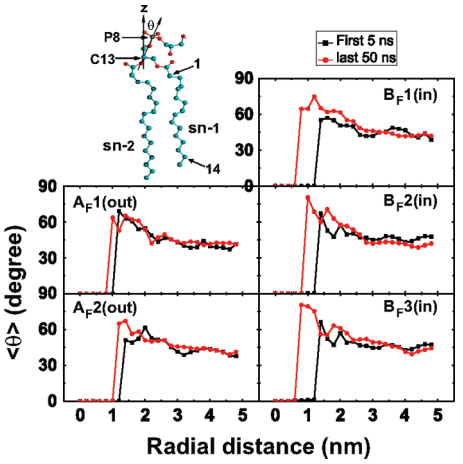

Figure 4. Time-averaged angle θ between the C13−P8 vector and the bilayer normal over the first 5 ns and the last 50 ns as a function of radial distance from the center of Aβ25−35 barrel for all the MD runs of A_F(out) and B_F(in) systems. The value of θ at zero is due to the fact that there are no lipid molecules within the barrel.

the angle (θ) between the vector from C13 in the lipid tail to P8 in the glycerol head and the bilayer normal (*z*-axis) (see the upper left panel of Figure 4). The average value of θ is ∼35° for a pure POPG bilayer. Figure 4 gives the time-averaged θ between the C13−P8 vector and *z*-axis over the last 50 ns as a function of radial distance from the center of Aβ25−35 barrel. The value of θ at zero at shorter distance is due to the fact that there are no lipid molecules within the barrel. It can be seen from Figure 4 that lipids closer to the Aβ25−35 barrel adopt a more tilted conformation in all the A_F(out) and B_F(in) MD runs. A considerable reorientation takes place for lipids in the three MD runs of B_F(in) system, with a maximum θ of ∼80° at radial distance around 1 nm, being much larger than the maximum θ in the two A_F(out) MD runs, showing again a larger membrane perturbation effect of barrel B(in) than barrel A(out). With the increase of the distance, the angle θ decreases and reaches a plateau of ∼40° at radial distance >2.5 nm, close to the θ value of ∼35° of a pure POPG bilayer, indicating Aβ25−35 barrel-like oligomers locally perturb the membrane ordering. Qualitatively similar results are obtained when the angle between *sn*-1 chain (from carbon atoms 2 to 13)

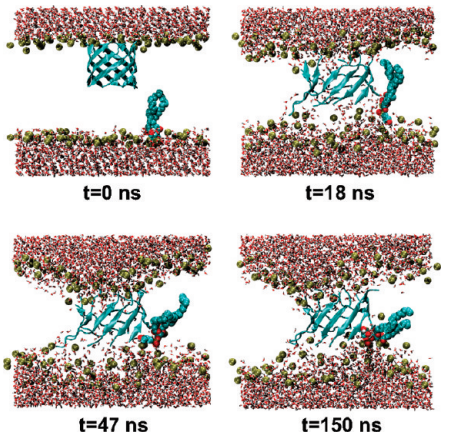

Figure 5. Snapshots in MD run B_F1(in) at four different time points. The oxygen atoms of water molecules and P atoms of lipid molecules are in red and tan, respectively. One representative lipid closer to the barrel is in vdW representation to illustrate its orientation change. For clarity, the hydrophobic tails of other POPG lipids are not shown.

and *z*-axis is used to describe the lipid orientation (data not shown). These results indicate that the lipids closer to Aβ25−35 barrel are strongly affected, which is consistent with what Tieleman et al. proposed that the lipids that interact strongly with the protein become increasingly tilted relative to the bilayer normal.[53] The tilting of the lipids induced by Aβ25−35 barrel can be also seen from the difference of the time-averaged angle θ between the last 50 ns and the first 5 ns for radial distance <2.5 nm. This reorientation allows the hydrophobic lipid tails to avoid being in contact with the penetrating water molecules.

The reorientation process of the lipids can be seen clearly from the configuration of one representative lipid closer to the barrel in the four representative snapshots in B_F1(in) trajectory (see Figure 5). Along this process, membrane perturbation and water penetration occur. At t = 0 ns, lipids in the two leaflets are well packed and there are no water molecules in the interior of the membrane. At t = 18 ns, a serious local deformation is observed for the lipids in the vicinity of Aβ25−35 β-barrel, opening up a region through which water can penetrate into the two entrances of the barrel. This is followed by an increase of the β-barrel diameter, leading to a larger hydrophilic channel for water molecules to enter. At t = 47 ns, a negative curvature is observed for the upper leaflet and the lipid becomes more titled with respect to the bilayer normal. With the increase of simulation time, the lipid gets more disordered. At t = 150 ns, it is almost perpendicular to the bilayer normal and the P atoms of a few of lipids diffuse to the center of the membrane. This leads to the relaxation of the hydrophilic pore toward a toroidal shape, which is lined by both Aβ25−35 peptides and lipid head groups. It is noted that during the process of toroidal pore formation, three out of eight β-strands lose their β-sheet content and the corresponding interpeptide backbone H-bonds break (see Figure S3 in the Supporting Information), leading to an increase of pore diameter to 0.35 nm from the initial value of 0.3 nm. Similar sizes of pores are observed in another two MD runs B_F2(in) and B_F3(in). Overall, the pore diameter ranges from 0.35 to 0.4 nm. This size of the pore allows water molecules to pass through as it was reported that a pore with a diameter of 0.23 nm is sufficiently large to allow water molecules along its whole length.[34] The partially disordered feature of Aβ25−35 pore is consistent with the recently proposed dynamic nature of β-sheet amyloid

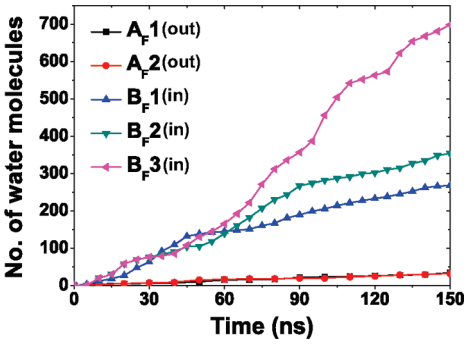

Figure 6. Time evolution of the accumulated number of water molecules across the bilayer for all the MD runs of A_F(out) and B_F(in) systems.

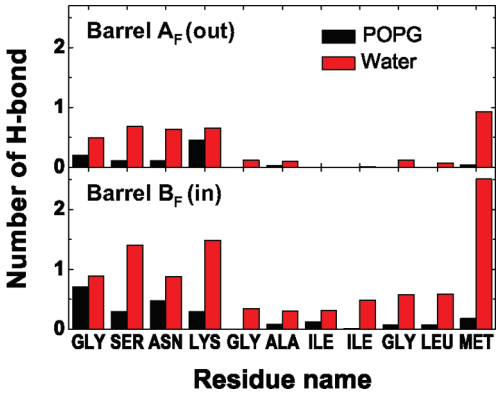

Figure 7. Time-averaged number of H-bonds of Aβ25−35−POPG and Aβ25−35−water (per peptide chain). The data in the MD runs of A_F1-2(out)/B_F1-3(in) have been used to calculate the average number of H-bonds between barrel A(out)/B(in) and solvents.

pore/channel based on multiple independent 30 ns MD simulations by Jang et al.[54−57]

In the snapshots shown in Figure 2, water molecules in the A_F(out) and B_F(in) systems are observed to penetrate into the hydrophobic region of the bilayer to different extents. To examine whether there are water molecules passing through the bilayer, we have calculated the accumulated number of water molecules across the lipid bilayers. Figure 6 shows the time evolution of the accumulated number of water molecules for each MD run of A_F(out) and B_F(in) systems. It is noted that there are no water molecules across the bilayer within the first 5 ns. At $t > 5$ ns, the number of water molecules increases steadily in the three B_F(in) MD runs. At $t = 150$ ns, it reaches to ∼270, 360, and 700 in B_F1(in), B_F2(in), and B_F3(in) MD trajectories, respectively. By carefully looking at the MD trajectories, we found that the transported water molecules are mostly through the inner side of barrel B. It is noted that there is no unidirectional water flux across the POPG bilayer. In the A_F(out) MD runs, the number of water molecules slowly reaches to ∼30 and keeps almost constant from 100 to 150 ns, indicating there are almost no water molecules passing through the bilayer during the last 50 ns of the simulations. Similar behavior is observed in the MD runs of all the other systems A_F(in), B_F(out), C_F(out), and C_F(in) (see Figure S4 in the Supporting Information). Trajectory visualization shows that water molecules are mostly trapped in the two entrances of barrel A(out) (see below for more detailed discussion). The different behaviors of water molecules attribute to the different conformations of the two barrels (see the conformations of A_F(out) and B_F(in) at $t = 0$ ns in Figure 1) and the corresponding different peptide−solvent interactions (see Figure S1 in the Supporting Information). In barrel A(out), Lys residues are located in the two entrances of the barrel (see Figure 1, A_F(out) at $t = 0$ ns), separated by hydrophobic residues with a distance of ∼1.4 nm, which is difficult for the charged side chains of Lys residues to form a continuous hydrophilic interface. The same is for A_F(in) (see Figure 1, A_F(in) at $t = 0$ ns). In addition, the initial state of barrel A(out) has a hydrophobic channel formed by the side chains of hydrophobic residues I31 and M35. The channel collapses very quickly due to the strong hydrophobic interactions, leading to a smaller pore with a diameter of 0.2 nm, which is too small to allow water molecules to go through.[34] Similar feature is observed for barrel B_F(out) and C_F(out). In contrast, in barrel B(in), the side chains of Lys residues are located on the inner side of the barrel and are close to each other (see Figure 1, B_F(in)), which is readily to form a hydrophilic channel. This arrangement facilitates water molecules to pass through barrel B(in) easily. The big difference of number of water molecules across the bilayer in B_F(in) and C_F(in) systems (see Figure 6 and Figure S4 in the Supporting Information) might be ascribed to the different arrangements of side chains inside the two barrels.

To elucidate the interactions of individual residues with the surrounding POPG lipid and water molecules, we have calculated the time-averaged number of H-bonds of Aβ25−35 β-barrel (per peptide chain) with lipid and water molecules (see Figure 7). The source of H-bond formation is electrostatic interactions between Aβ25−35 peptide with the charged head groups of POPG lipids and with water molecules. As depicted in Figure 7, the N-terminal polar residues Ser26-Asn27-Lys28 both in A_F(out) and B_F(in) systems show a relatively high hydrogen-bonding propensity with water and lipid molecules, indicating the existence of strong electrostatic interactions between these residues and the solvents. A big difference of H-bonding propensity with surrounding solvents is observed for the hydrophobic residues Ala30-Ile31-Ile32-Gly33-Leu34: almost no H-bonds for A_F(out) but more H-bonds for B_F(in). These results indicate that water molecules are trapped in the two entrances of barrel A(out) but penetrate into the center of barrel B(in), consistent with the results by trajectory visualization. As it is impossible for the nonpolar tails of the lipids to form H-bonds with Aβ25−35 due to their lack of H-bond donor/acceptor, the formation of H-bonds between the head groups of lipids and Ala30-Ile31 located in the middle of barrel B(in) elucidates again the tilting of lipid molecules as well as the formation of toroidal-shaped amyloid pores. It is noted that the high hydrogen-bonding propensity with water molecules for the two terminal residues G25 and M35 is due to the diffusion of water molecules into the two entrances of barrel A(out) and B(in). During the whole MD trajectories, Leu34 are observed to stay inside the lipid bilayer, consistent with the results by the technique of neutron diffraction and selective peptide deuteration that the deuterated amino acid Leu34 of Aβ25−35 is located in the hydrophobic core of the lipid bilayer.[58]

In order to examine the preference of barrel B(in) for staying inside the hydrophobic core of the POPG bilayer, we have carried out MD simulations by partially inserting barrel A(out) and B(in) in the bilayer (see A_P1(out) and B_P1(in) in Figure 8a). Similar strategy was used previously in a 50 ns MD simulation study on the insertion of an antimicrobial peptide into a lipid bilayer.[59]

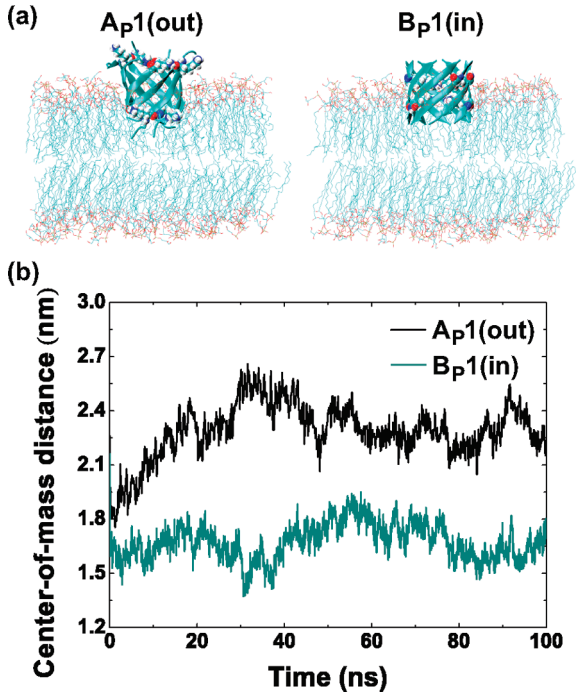

Figure 8. Initial states of MD runs A_P1(out) and B_P1(in) for partial-insertion systems (a) and the time evolution of the COM distance between the C_α atom of Aβ25−35 β-barrel and the P atom of POPG lipid bilayer in A_P1(out) and B_P1(in) MD runs of the partial-insertion system (b).

Partial Insertion of Aβ25−35 β-Barrel Results in a Tendency To Stay Inside for Barrel B(in). The interactions between Aβ25−35 β-barrel-like oligomer and a POPG lipid bilayer are studied for the partial-insertion systems A_P(out) and B_P(in). By looking at the MD trajectories, we observed that barrel A(out) has a tendency to be expelled from the bilayer, while barrel B(in) prefers to stay inside. The different behavior of Aβ25−35 β-barrels is monitored by the time evolution of their positions with respect to the lipid bilayer. Figure 8b shows the center of mass (COM) distance between C_α atoms of β-barrel and P atoms of the POPG lipid bilayer as a function of time. It is noted that the COM distance is zero when Aβ25−35 is located in the center of the bilayers. The initial COM distance is ∼2.0 nm for A_P1(out) and B_P1(in) MD runs, indicating that the Aβ25−35 β-barrel is partially inserted in the POPG lipid bilayers. Within the first 200 ps, barrel A(out) and barrel B(in) both insert deeply into the bilayer, reaching to a COM distance of 1.8 and 1.7 nm, respectively. This fast decrease of the COM distance might be driven by the strong hydrophobic interactions between lipid tails and the hydrophobic residues of Aβ25−35. From 200 ps to 18 ns, the two COM distances increase to 2.4 and 1.8 nm, respectively, indicating that the two barrels both move toward the bilayer surface. From 18 to 30 ns, barrel A(out) continues moving to the surface, while barrel B(in) moves down to the center of the bilayer. After that, the COM distance of barrel A(out)/B(in) with respect to the lipid bilayer fluctuates around 2.2 and 1.6 nm, suggesting that barrel A(out) has a trend to exit the bilayer, while barrel B(in) has a tendency to insert deeply and stay inside the bilayer. It is expected that much longer simulation is needed for barrel B(in) to insert completely into the bilayer. The observed behavior of barrel B staying inside the lipid bilayer is consistent with previous experimental studies by using small-angle X-ray diffraction[27] and neutron diffraction techniques.[28] The small-angle X-ray diffraction pattern analysis shows that Aβ25−35 is highly lipophilic and inserts into the membrane hydrocarbon core[27] and the neutron diffraction analysis demonstrates that Aβ25−35 inserts quite deeply in the bilayer core of anionic lipid membranes.[28] It should be noted that membrane leakage is not observed in the two partial-insertion systems.

The different tendency of barrel A(out)/B(in) to move to the surface/center of the bilayer is further analyzed by the probability distribution of interaction energies of Aβ25−35 β-barrel (barrel A(out) and barrel B(in)) with surrounding POPG lipid molecules (see Figure S5 in the Supporting Information). The total interaction energy of membrane−barrel B(in) is ∼350 kJ/mol lower than that of membrane--barrel A(out), indicating that it is energetically favorable for barrel B(in) staying inside the POPG bilayer. The contribution of the electrostatic and vdW interactions to the total interaction energies is different for A_P1(out) and B_P1(in) systems. The electrostatic interactions are dominant in barrel A(out), while in barrel B(in) they are weaker than the vdW interactions

DISCUSSION AND CONCLUSIONS

The interactions of several disease-related peptides/proteins (including Aβ, α-synuclein, islet amyloid polypeptide−IAPP, and prion protein) with membranes have received considerable attention[60−64] due to their important role in cytotoxicity. These amyloidogeneric peptides have been reported to form pore-/channel-like structures in membrane, causing membrane disruption and leakage.[14,16,65−68] The observation of pores/channels among such a diverse variety of peptide sequences suggests an underlying similarity in the physical chemical structures involved. Among these peptides, Aβ and its shorter fragments are the most extensively studied systems experimentally.[10,14,15,17,23,25,26] Computationally, the insertion behavior, the stability of preinserted, and the structure of surface-bound Aβ monomer have been studied by Monte Carlo simulations in implicit membrane[69] and by MD simulations in explicit membrane.[70−72] Helical and random coil structures are observed for the preinserted and surface-bound states, respectively. Recent all-atom MD simulations on modeled Aβ9−42/Aβ11−42/Aβ17−42 pores/channels consisting of solid-state NMR-based U-shaped β-strand-turn-β-strand motif show that the pore/channels are water-/ion-permeable and present mobile β-sheet subunits.[54,55,57,73] Those studies have provided significant insight into the monomeric and oligomeric structures of Aβ (including Aβ9−42, Aβ11−42, Aβ17−42, and full-length Aβ1−40/1−42) in membrane and their membrane perturbation effect. Compared to the structural studies of the longer Aβ segments, the naturally produced 11-residue Aβ25−35 fragment is less investigated computationally.

Our multiple independent 150 ns MD simulations of the six preformed eight-stranded Aβ25−35 β-barrel conformations (A(out), A(in), B(out), B(in), C(out), and C(in)) in an anionic POPG bilayer demonstrate that barrel B and barrel A/C interact differently with the POPG bilayer. The former affects strongly the local structure of membrane and forms water-permeable pore in toroidal shape when Lys residues are located on the inner side of the barrel. We further estimate the relative stabilities of these barrels based on the Boltzmann probabilities of the barrel-like octamers obtained in the MD simulations by using a Monte Carlo method described in the Analysis subsection. For A_F(out)/B_F(in) systems, the conformational energy used for the probability

calculation is averaged over the two/three independent MD runs. The evaluated Boltzmann probabilities for A(out), A(in), B(out), B(in), C(out), and C(in) are 8%, 20%, 28%, 25%, 16%, and 3%, respectively. These results suggest that all these barrels are marginally populated inside POPG bilayer, while B(out) and B(in) barrels are the most populated ones. Together with the accumulated number of water molecules across the bilayer shown in Figure 6 and Figure S4 (in the Supporting Information), we propose that barrel B(in) is the most likely Aβ25−35 pore/channel structure which leads to membrane leakage.

The toroidal-shaped pore/channel has also been observed for protegrin-1 toxin in a previous MD study by Jang et al.,[74] but barrel-stave pore/channel observed for Aβ9−42 peptide.[57] Lashuel and Lansbury[75] reported the AFM images of Aβ oligomers that are arranged in pore shapes and appear to resemble pore structures similar to those formed by oligomeric membrane-lysing β-sheet bacteria toxins such as α-hemolysin.[76] Most of these pore-forming bacteria toxins form β-barrel-like pores and are 1.0−3.5 nm in diameter.[77,78] Which membrane pore type that the amyloid peptides form might depend on the outward-facing amino acid sequence interacting with the bilayer.[57] Quist et al. presented the AFM images of individual porelike structure of several disease-related amyloid peptides, including Aβ1−40, α-synuclein, British amyloid (ABri), Danish amyloid (ADan), serum amyloid A (SAA), and IAPP in membrane. Although the AFM images could not provide detailed information on the conformations (owing to their relatively low resolution), porelike structures with various sizes were clearly observed. The diameters of such cavity pores are 1−2 nm,[16] similar to the diameters of some bacteria toxin pores. In the present study, eight-stranded Aβ25−35 β-barrel is considered as a model system to investigate the first step interaction mechanism of Aβ25−35 β-barrel-like oligomer with a POPG lipid bilayer. The Aβ25−35 porelike oligomers generated in our MD simulations have diameters of 0.35—0.4 nm. Although they are much smaller than the amyloid pores measured from AFM images,[16] our MD simulations show that they are water-permeable. Further studies are needed to explore the interactions of anionic lipid bilayer with larger Aβ25−35 porelike oligomers with diameter similar to those from AFM images.

Different mechanisms have been proposed to be involved in the amyloid oligomer-mediated membrane permeability: pore/channel formation[16,75] and membrane destabilization.[79,80] Our MD simulations show that Aβ25−35 β-barrel-like oligomers with Lys residues on its inner side has a preference to stay inside the POPG bilayer and forms a porelike structure that perturbs the local structure of membrane and causes membrane leakage. It seems that the mechanism of Aβ25−35 β-barrel-like oligomer-mediated membrane permeability involves both pore formation and membrane destabilization.

The interactions of Aβ25−35 β-barrel with a POPG bilayer not only perturb the local membrane structure but also change the conformations of Aβ25−35 β-barrel-like oligomers. Figure S3 (in the Supporting Information) shows the time evolution of secondary structure profile and the number of interpeptide H-bonds of barrel B(in) when it is fully inserted in the bilayer. Loss of β-sheet content for some of the peptide chains is observed in all the MD runs. A decrease of number of H-bonds occurs in B_F2(in) and B_F3(in) MD runs. However, the loss of β-sheet content does not necessarily occur concomitantly with the breaking of interpeptide H-bonds. In B_F1(in) trajectory, the number of H-bonds keeps constant during the whole process of simulations.

The results of our MD simulations provide significant insight toward the atomic resolution structure of Aβ25−35 β-sheet-rich pores and the disruption of pores on the membrane permeability. It is noted that the POPG bilayers used in this study are only simplified models of the complex lipid and cholesterol mixtures of which cellular membranes are composed. A more complicated model such as mixed POPC/POPG or POPE/POPG membrane could mimic the cellular membrane better. However, the effects of the model bilayer on the main results obtained from this study could be eliminated to a large extent when the comparison of interactions of lipid bilayer with barrel B and barrel A/C is concerned. Therefore, the POPG model bilayer does provide a simplified but appropriate system for investigating the interactions of Aβ25−35 β-barrel-like oligomer with biological membrane and the membrane perturbation mechanism of Aβ25−35 oligomers at the atomic levels.

In conclusion, we have investigated the detailed interactions of six preformed Aβ25−35 barrel-like octamers (A(out), A(in), B(out), B(in), C(out), and C(in)) with the anionic POPG bilayer and the resulting membrane perturbation. Our extensive MD simulations provide atomic resolution model for Aβ25−35 β-sheet-rich pores/channels. The structure feature of Aβ25−35 β-barrel-like pores is consistent with the one proposed by Kagan et al.[24,26,29] As amyloid pores/channels are not present in a unique size and can vary in size, shape, and morphology in membrane,[14−16] other Aβ25−35 pore models are also possible. Our multiple 150 ns MD runs show that barrel B(in) strongly affects the local ordering of the POPG lipid bilayer and forms water-permeable pore in toroidal shape. The observed β-sheet-rich Aβ25−35 pore is partially disordered with H-bonds broken in some regions. This observation is consistent with the recently proposed dynamic nature of Aβ9−42/Aβ11−42/Aβ17−42 amyloid pore/channel by Jang et al.[54,55,57] Moreover, it is known that β-barrels that span the membrane typically comprise 8−22 β-strands (each 10−13 residues long).[33] As Aβ25−35 is composed of 11 residues, the β-barrels formed by this peptide can span the membrane. Our MD simulation results together with previous experimental studies by Kagan et al.[24,26,29] suggest that β-barrel-like oligomer with the side chains of Lys located on the inner side of the barrel is the most likely Aβ25−35 pore/channel structure leading to membrane leakage. Such an Aβ25−35 β-barrel-like pore, with most hydrophilic residues protected from the membrane, might form in the membrane after the insertion of monomer, as proposed by Lin et al. for the formation of Aβ42 annular pores.[14]

■ ASSOCIATED CONTENT

Supporting Information. The five figures report the time evolution of the interaction energy of Aβ25−35 β-barrel with surrounding solvent (POPG+water) molecules for A_F(out) and B_F(in) systems (Figure S1); the time-averaged order parameter S_{CD} of *sn*-1 chain of lipids in the MD runs of A_F(in), B_F(out), C_F(in), and C_F(out) system (Figure S2); the secondary structure profile of Aβ25−35 β-barrel and the number of interpeptide backbone H-bonds in the three MD runs of B_F(in) system (Figure S3); the time evolution of the accumulated number of water molecules across the bilayer in the MD runs of A_F(in), B_F(out), C_F(in), and C_F(out) system (Figure S4); the probability distribution of the interaction energy of Aβ25−35 β-barrel with

POPG molecules in the MD runs of A_P(out) and B_P(in) system (Figure S5). This material is available free of charge via the Internet at http://pubs.acs.org.

AUTHOR INFORMATION

Corresponding Author

*Tel: (86) 21 55665231. Fax: (86) 21 65104949. E-mail: ghwei@fudan.edu.cn.

ACKNOWLEDGMENT

We thank Dr. Buyong Ma for careful reading and constructive comments on the manuscript. This work was supported by the National Natural Science Foundation of China (Grant No. 11074747), Research Fund for the Doctoral Program of Higher Education of China (RFDP-20100071110006), and the Program for New Century Excellent Talents in University (NCET-08-0125). Simulations were performed at the Shanghai Supercomputing Center and the National High Performance Computing Center of Fudan University.

REFERENCES

(1) Selkoe, D. J. *Nature* **1999,** *399*, A23.
(2) Barrow, C. J.; Yasuda, A.; Kenny, P. T.; Zagorski, M. G. *J. Mol. Biol.* **1992,** *225*, 1075.
(3) Lesne, S.; Koh, M. T.; Kotilinek, L.; Kayed, R.; Glabe, C. G.; Yang, A.; Gallagher, M.; Ashe, K. H. *Nature* **2006,** *440*, 352.
(4) Hung, L. W.; Ciccotosto, G. D.; Giannakis, E.; Tew, D. J.; Perez, K.; Masters, C. L.; Cappai, R.; Wade, J. D.; Barnham, K. J. *J. Neurosci.* **2008,** *28*, 11950.
(5) Onoa, K.; Condron, M. M.; Teplow, D. B. *Proc. Natl. Acad. Sci. U.S.A.* **2009,** *106*, 14745.
(6) Demuro, A.; Mina, E.; Kayed, R.; Milton, S. C.; Parker, I.; Glabe, C. G. *J. Biol. Chem.* **2005,** *280*, 17294.
(7) Arispe, N.; Pollard, H. B.; Rojas, E. *Ann. N.Y. Acad. Sci.* **1994,** *747*, 256.
(8) Arispe, N.; Rojas, E.; Pollard, H. B. *Proc. Natl. Acad. Sci. U.S.A.* **1993,** *90*, 567.
(9) Arispe, N.; Pollard, H. B.; Rojas, E. *Proc. Natl. Acad. Sci. U.S.A.* **1993,** *90*, 10573.
(10) Alarcon, J. M.; Brito, J. A.; Hermosilla, T.; Atwater, I.; Mears, D.; Rojas, E. *Peptides* **2006,** *27*, 95.
(11) Arispe, N.; Pollard, H. B.; Rojas, E. *Proc. Natl. Acad. Sci. U.S.A.* **1996,** *93*, 1710.
(12) Rhee, S. K.; Quist, A. P.; Lal, R. *J. Biol. Chem.* **1998,** *273*, 13379.
(13) Hirakura, Y.; Lin, M. C.; Kagan, B. L. *J. Neurosci. Res.* **1999,** *57*, 458.
(14) Lin, H.; Bhatia, R.; Lal, R. *FASEB J.* **2001,** *15*, 2433.
(15) Kagan, B. L.; Hirakura, Y.; Azimov, R.; Azimova, R.; Lin, M. C. *Peptides* **2002,** *23*, 1311.
(16) Quist, A.; Doudevski, I.; Lin, H.; Azimova, R.; Ng, D.; Frangione, B.; Kagan, B.; Ghiso, J.; Lal, R. *Proc. Natl. Acad. Sci. U.S.A.* **2005,** *102*, 10427.
(17) Capone, R.; Quiroz, F. G.; Prangkio, P.; Saluja, I.; Sauer, A. M.; Bautista, M. R.; Turner, R. S.; Yang, J.; Mayer, M. *Neurotox. Res.* **2009,** *16*, 1.
(18) Kagan, B. L. *Science* **2005,** *307*, 42.
(19) Lau, T. L.; Ambroggio, E. E.; Tew, D. J.; Cappai, R.; Masters, C. L.; Fidelio, G. D.; Barnham, K. J.; Separovic, F. *J. Mol. Biol.* **2006,** *356*, 759.
(20) de Planque, M. R.; Raussens, V.; Contera, S. A.; Rijkers, D. T.; Liskamp, R. M.; Ruysschaert, J. M.; Ryan, J. F.; Separovic, F.; Watts, A. *J. Mol. Biol.* **2007,** *368*, 982.
(21) Gowing, E.; Roher, A. E.; Woods, A. S.; Cotter, R. J.; Chaney, M.; Little, S. P.; Ball, M. J. *J. Biol. Chem.* **1994,** *269*, 10987.
(22) Kubo, T.; Nishimura, S.; Kumagae, Y.; Kaneko, I. *J. Neurosci. Res.* **2002,** *70*, 474.
(23) Kaminsky, Y. G.; Marlatt, M. W.; Smith, M. A.; Kosenko, E. A. *Exp. Neurol.* **2010,** *221*, 26.
(24) Mirzabekov, T.; Lin, M. C.; Yuan, W. L.; Marshall, P. J.; Carman, M.; Tomaselli, K.; Lieberburg, I.; Kagan, B. L. *Biochem. Biophys. Res. Commun.* **1994,** *202*, 1142.
(25) Pike, C. J.; Walencewicz-Wasserman, A. J.; Kosmoski, J.; Cribbs, D. H.; Glabe, C. G.; Cotman, C. W. *J. Neurochem.* **1995,** *64*, 253.
(26) Lin, M. C.; Kagan, B. L. *Peptides* **2002,** *23*, 1215.
(27) Mason, R. P.; Estermyer, J. D.; Kelly, J. F.; Mason, P. E. *Biochem. Biophys. Res. Commun.* **1996,** *222*, 78.
(28) Dante, S.; Hauss, T.; Dencher, N. A. *Biophys. J.* **2002,** *83*, 2610.
(29) Mirzabekov, T.; Lin, M. C.; Kagan, B. L. *Biophys. J.* **1994,** *66*, A430.
(30) Lin, M. C.; Mirzabekov, T.; Kagan, B. L. *Biophys. J.* **1995,** *68*, A383.
(31) Ma, B.; Nussinov, R. *Biophys. J.* **2004,** *86*, 373A.
(32) Fu, Z.; Luo, Y.; Derreumaux, P.; Wei, G. *Biophys. J.* **2009,** *97*, 1795.
(33) Heuck, A. P.; Tweten, R. K.; Johnson, A. E. *Biochemistry* **2001,** *40*, 9065.
(34) Smart, O. S.; Neduvelil, J. G.; Wang, X.; Wallace, B. A.; Sansom, M. S. *J. Mol. Graph.* **1996,** *14*, 354.
(35) Elmore, D. E. *FEBS Lett.* **2006,** *580*, 144.
(36) Kandt, C.; Ash, W. L.; Tieleman, D. P. *Methods* **2007,** *41*, 475.
(37) Lindahl, E.; Hess, B.; van der Spoel, D. *J. Mol. Model* **2001,** *7*, 306.
(38) Friesner, R. A.; Tirado-Rives, J.; Jorgensen, W. L. *J. Phys. Chem. B* **2001,** *105*, 6474.
(39) Berger, O.; Edholm, O.; Jahnig, F. *Biophys. J.* **1997,** *72*, 2002.
(40) Tieleman, D. P.; et al. *J. Phys.: Condens. Matter* **2006,** *18*, S1221.
(41) Bjelkmar, P.; Niemelä, P. S.; Vattulainen, I.; Lindahl, E. *PLoS Comput. Biol.* **2009,** *5*, e1000289.
(42) Berendsen, H. J. C.; Postma, J. P. M.; Gunsteren, W. F. v.; Hermans, J. *Intermolecular Forces, Interaction models for water in relation to protein hydration*; D. Reidel Publishing Co., Dordrecht, The Netherlands, 1981; p 331.
(43) Hess, B.; Bekker, H.; Berendsen, H. J. C.; Fraaije, J. G. E. M. *J. Comput. Chem.* **1997,** *18*, 1463.
(44) Miyamoto, S.; Kollman, P. A. *J. Comput. Chem.* **1992,** *13*, 952.
(45) Darden, T.; York, D.; Pedersen, L. *J. Chem. Phys.* **1993,** *98*, 10089.
(46) Patra, M.; Karttunen, M.; Hyvonen, M. T.; Falck, E.; Lindqvist, P.; Vattulainen, I. *Biophys. J.* **2003,** *84*, 3636.
(47) Wiedmann, T.; Salmon, A.; Wong, V. *Biochim. Biophys. Acta* **1993,** *1167*, 114.
(48) Tolokh, I. S.; Vivcharuk, V.; Tomberli, B.; Gray, C. G. *Phys. Rev. E: Stat., Nonlinear, Soft Matter Phys.* **2009,** *80*, 031911.
(49) Vermeer, L. S.; de Groot, B. L.; Reat, V.; Milon, A.; Czaplicki, J. *Eur. Biophys. J.* **2007,** *36*, 919.
(50) Kabsch, W.; Sander, C. *Biopolymers* **1983,** *22*, 2577.
(51) Humphrey, W.; Dalke, A.; Schulten, K. *J. Mol. Graph.* **1996,** *14*, 33.
(52) Ma, B.; Levine, A. J. *Nucleic Acids Res.* **2007,** *35*, 7733.
(53) Tieleman, D. P.; Forrest, L. R.; Sansom, M. S.; Berendsen, H. J. *Biochemistry* **1998,** *37*, 17554.
(54) Jang, H.; Zheng, J.; Nussinov, R. *Biophys. J.* **2007,** *93*, 1938.
(55) Jang, H.; Zheng, J.; Lal, R.; Nussinov, R. *Trends Biochem. Sci.* **2008,** *33*, 91.
(56) Mustata, M.; Capone, R.; Jang, H.; Arce, F. T.; Ramachandran, S.; Lal, R.; Nussinov, R. *J. Am. Chem. Soc.* **2009,** *131*, 14938.
(57) Jang, H.; Arce, F. T.; Capone, R.; Ramachandran, S.; Lal, R.; Nussinov, R. *Biophys. J.* **2009,** *97*, 3029.
(58) Dante, S.; Hauss, T.; Dencher, N. A. *Biochemistry* **2003,** *42*, 13667.
(59) Soliman, W.; Bhattacharjee, S.; Kaur, K. *Langmuir* **2009,** *25*, 6591.
(60) Verdier, Y.; Zarandi, M.; Penke, B. *J. Peptide Sci.* **2004,** *10*, 229.

(61) Jao, C. C.; Der-Sarkissian, A.; Chen, J.; Langen, R. *Proc. Natl. Acad. Sci. U.S.A.* **2004,** *101*, 8331.
(62) Janson, J.; Ashley, R. H.; Harrison, D.; McIntyre, S.; Butler, P. C. *Diabetes* **1999,** *48*, 491.
(63) Dupiereux, I.; Zorzi, W.; Lins, L.; Brasseur, R.; Colson, P.; Heinen, E.; Elmoualij, B. *Biochem. Biophys. Res. Commun.* **2005,** *331*, 894.
(64) Simakova, O.; Arispe, N. J. *J. Neurosci.* **2007,** *27*, 13719.
(65) Lashuel, H. A.; Petre, B. M.; Wall, J.; Simon, M.; Nowak, R. J.; Walz, T.; Lansbury, P. T., Jr. *J. Mol. Biol.* **2002,** *322*, 1089.
(66) Kayed, R.; Sokolov, Y.; Edmonds, B.; McIntire, T. M.; Milton, S. C.; Hall, J. E.; Glabe, C. G. *J. Biol. Chem.* **2004,** *279*, 46363.
(67) Kagan, B. L.; Azimov, R.; Azimova, R. *J. Membr. Biol.* **2004,** *202*, 1.
(68) Lal, R.; Lin, H.; Quist, A. P. *Biochim. Biophys. Acta* **2007,** *1768*, 1966.
(69) Mobley, D. L.; Cox, D. L.; Singh, R. R.; Maddox, M. W.; Longo, M. L. *Biophys. J.* **2004,** *86*, 3585.
(70) Xu, Y.; Shen, J.; Luo, X.; Zhu, W.; Chen, K.; Ma, J.; Jiang, H. *Proc. Natl. Acad. Sci. U.S.A.* **2005,** *102*, 5403.
(71) Lemkul, J. A.; Bevan, D. R. *Arch. Biochem. Biophys.* **2008,** *470*, 54.
(72) Davis, C. H.; Berkowitz, M. L. *J. Phys. Chem. B* **2009,** *113*, 14480.
(73) Jang, H.; Arce, F. T.; Ramachandran, S.; Capone, R.; Azimova, R.; Kagan, B. L.; Nussinov, R.; Lal, R. *Proc. Natl. Acad. Sci. U.S.A.* **2010,** *107*, 6538.
(74) Jang, H.; Ma, B.; Woolf, T. B.; Nussinov, R. *Biophys. J.* **2006,** *91*, 2848.
(75) Lashuel, H. A.; Lansbury, P. T., Jr. *Q. Rev. Biophys.* **2006,** *39*, 167.
(76) Czajkowsky, D. M.; Sheng, S.; Shao, Z. *J. Mol. Biol.* **1998,** *276*, 325.
(77) Song, L.; Hobaugh, M. R.; Shustak, C.; Cheley, S.; Bayley, H.; Gouaux, J. E. *Science* **1996,** *274*, 1859.
(78) Petosa, C.; Collier, R. J.; Klimpel, K. R.; Leppla, S. H.; Liddington, R. C. *Nature* **1997,** *385*, 833.
(79) Sokolov, Y.; Kozak, J. A.; Kayed, R.; Chanturiya, A.; Glabe, C.; Hall, J. E. *J. Gen. Physiol.* **2006,** *128*, 637.
(80) Dante, S.; Hauss, T.; Brandt, A.; Dencher, N. A. *J. Mol. Biol.* **2008,** *376*, 393.